Electrical Impedance Tomography

Andy Adler and Alistair Boyle

Carleton University, Ottawa, Canada

Abstract: Electrical Impedance Tomography (EIT) is a medical imaging technique which uses electrical stimulations and measurements at body-surface electrodes. From these data, images of the distribution of conductivity within the body are calculated by solving an inverse problem. EIT has the advantage of producing high temporal resolution data, while being relatively low cost, non-invasive, small, and not using ionizing radiation. On the other hand, EIT has disadvantages in providing low spatial resolution, and being sensitive to changes at the electrodes. EIT is currently being used clinically for monitoring of ventilated patients, and is also being actively researched for applications such as cardiovascular flows and pressures, brain and nervous activity, cancer screening, and monitoring of gastrointestinal flows. EIT is similar to the electrical resistance tomography used in geophysical and process monitoring. This article reviews EIT from the point of view of its applications as well as image generation and interpretation.

1   Introduction

Electrical Impedance Tomography (EIT) is an imaging technique which estimates the distribution of electrical properties (and their changes over time) within a body. EIT systems make electrical stimulations and measure the voltages at combinations of body surface electrodes, from which images are reconstructed.

EIT is useful when contrasts in electrical properties of tissue correspond to clinically interesting conditions, such as air movement in the lungs, or the presence of cancerous tissues. For example, figure 1 shows the application of EIT for monitoring of breathing in a newborn. EIT measurements are non-invasive, and use no ionizing radiation; it is capable of high temporal resolution, and is potentially inexpensive, using commodity electronics components. On the other hand, EIT has poor spatial resolution and can be sensitive to artefacts due to electrode effects.

The name EIT derives from the fact that electrical impedance measurements are the source data for the tomographic images. The reconstructed images are in units of impedivity (or resistivity if at low frequency) – not impedance. EIT is a "tomographic" modality in the sense that it creates images of the internal properties of the body; however, EIT is different from the true tomographic imaging methods in that slices cannot be imaged independently, due to the diffuse propagation of electrical current.

EIT is primarily used for medical applications. However, it is closely related to electrical resistance tomography (ERT) which is used for geophysical imaging and in process tomography. EIT is also related to impedance spectroscopy – characterizing the impedance spectrum (i.e. as a function of stimulation frequency) of a sample. The primary difference is that impedance spectroscopy uses one pattern of stimulus and measurement electrodes,
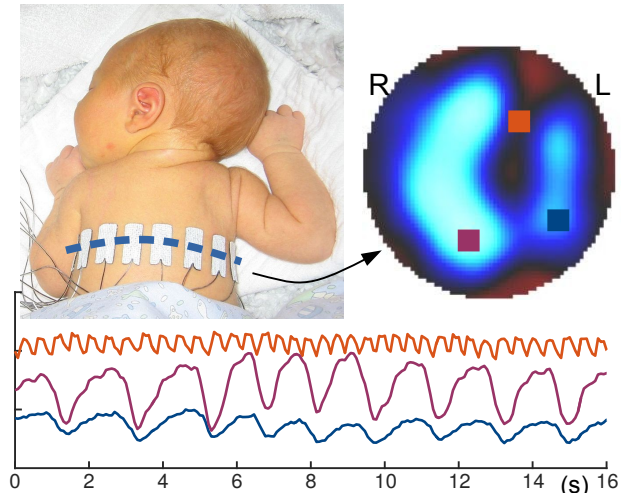
Figure 1: A 10-day old infant with EIT electrodes, from the study (56), from which cross-sectional images are reconstructed with pixel waveforms showing the heart and left and right lung activity. For an infant with the head turned to the side, the contralateral lung receives most tidal ventilation.

and does not calculate images. EIT can thus be seen as an imaging extension of impedance spectroscopy.

The earliest reference to the concepts behind medical EIT were for geophysical imaging, by Schlumberger in 1911 (12). For medical imaging, EIT was introduced by Henderson and Webster (57) in the late 1970s followed by the work of Barber and Brown in the early 1980s (15). Early work focused on imaging of the lungs and heart, with subsequent development toward imaging of the abdomen, brain, and breast. Work in the geophysical domain, has progressed largely independently of medical developments; ERT currently sees most application for
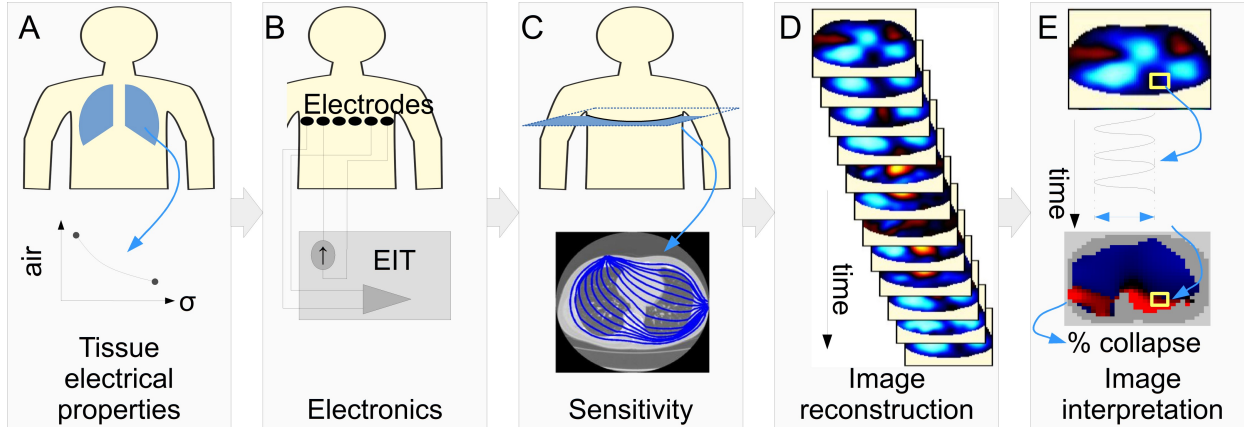
Figure 2: Overview of the steps in EIT image generation and interpretation, from (47). A: physiologically interesting tissues have electrical properties which contrast with surrounding tissues or change over time; B: EIT hardware systems apply electrical current and measures voltages on a sequence of body surface electrodes; C: The pattern of electrical stimulation and measurements, and the body geometry and electrical properties, determine the sensitive region; D: Images of the conductivity (absolute EIT) or the change in conductivity (difference EIT) are calculated by using the sensitivity field in an image reconstruction algorithm; and E: Physiologically relevant measures are calculated from image contrasts and their changes over time.

imaging of conductive (i.e. metal-bearing) ore and the presence and movement of liquids (e.g. for groundwater and leaching). Another application area for imaging of impedance has been in the process tomography community, for imaging the flow and mixing of industrial fluids (16).

Mathematical interest in the inverse problem was kindled by the work of Calderón (27) in 1980, with work focusing on the existence and uniqueness of EIT solutions (89). Currently, medical EIT systems are manufactured by several companies (47) for human and veterinary use, with the primary application of monitoring breathing. A broad research community has formed, meeting annually at the "International Conference on Biomedical Applications of Electrical Impedance Tomography." Much of the software and data is available in an open source project, EIDORS (3). A number of good overviews of EIT applications have been written, to which we refer the interested reader: (5, 9, 7, 17, 35, 47, 46, 43, 59, 64, 67, 75, 81).

The remainder of this article is organized as follows: in section 2, we describe applications of EIT, with a more detailed description of two applications. The subsequent sections describe EIT image generation and reconstruction, as illustrated in figure 2. First, a phenomenon of interest creates a contrast in the electrical properties of tissue (section 3); for example the movement of air into the lungs decreases the conductivity of lung tissue in proportion to the quantity of air received, while the conductivity spectrum of cancerous tissue contrasts with surrounding tissues. To measure electrical properties, EIT uses body surface electrodes, through which applied currents (or for some systems, voltages) are applied and volt-

ages measured (section 4). The sensitivity and resolution of EIT (section 5) is determined by the electrode number and position, as well as the selection and sequence of electrodes onto which stimulus and measurements are applied. Using the measured data, EIT images are reconstructed, using a variety of imaging algorithms (section 6). Finally, based on the reconstructed EIT images, measures of the underlying physiological parameters are calculated. Many approaches to image analysis have been developed (section 7) including functional EIT (fEIT) approaches which look at the temporal evolution of the EIT voxel waveforms. Table 1 defines terminology used in this article.

2   EIT Applications

In this section, we review two example applications (detection of cancerous regions in breast tissue using frequency-difference EIT, and imaging of breathing using time-difference EIT), and then provide a more complete list of applications and relevant references.

The impedance of tissues increases as a function of frequency and these impedance spectra are characterized by "dispersions" where current is able to cross membranes (section 3). Cancerous tissue often has a different impedance spectrum from non-malignant tissues, largely due to the increased blood flow (angiogenesis), and the increased density of tumour stroma (61).

The next example shows EIT for monitoring of the distribution of gas during breathing. For patients using a mechanical ventilator, there is a concern that the lower (dependent) lung regions could become collapsed, so that all
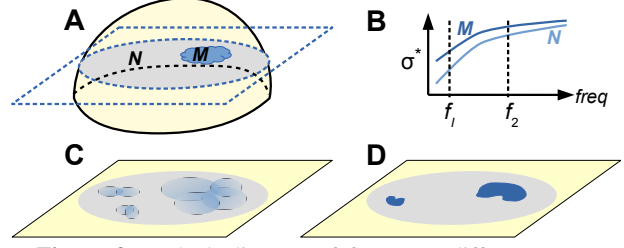
Table 1: Terminology Used

Term	Definition
A/D	Analog to digital converter
CEM	Complete electrode model
CMRR	Common-mode rejection ratio
COPD	Chronic obstructive pulmonary disease
D/A	Digital to analog converter
EIT	Electrical Impedance Tomography
fEIT	functional EIT
FEM, $F(\cdot)$	Finite Element Model
FVC	Forced Vital Capacity
FEV_1	Forced Expiratory Volume in 1 s
FPGA	Field-programmable gate array
$\mathbf{J}$	Jacobian matrix: $\partial \mathbf{y}_i / \partial \mathbf{x}_j$
$\mathbf{I}$	Applied current patterns $\in \mathbb{R}^{N_E \times N_C}$
λ	Hyperparameter for reconstruction
$\mathbf{M}$	Mapping from inverse to forward models
$\mathcal{N}(\cdot, \cdot)$	Distributed with mean, covariance
N_E	Number of Electrodes
N_C	Number of Current patterns
N_F	Number of elements in FEM
TV	Tidal Volume (breathing) *or* Tidal Variation (EIT) *or* Total Variation (imaging)
τ	Time constant
DC	Direct current (zero frequency)
$p(\cdot)$	Probability of $\cdot$
$\mathbf{Q}$	Image prior distribution $\propto \boldsymbol{\Sigma}_x^{-1}$
$\mathbf{R}$	Linear reconstruction matrix: $\hat{\mathbf{x}} = \mathbf{R}\mathbf{y}$
$\boldsymbol{\sigma}, \boldsymbol{\sigma}_r, \boldsymbol{\sigma}_F$	Conductivity distribution. $\cdot_r$: at reference time. $\cdot_F$: on forward model.
σ	standard deviation (scalar)
$\boldsymbol{\Sigma}_n, \boldsymbol{\Sigma}_x$	Covariance. $\cdot_n$: of noise, $\cdot_x$: of image prior.
$\mathbf{W}$	Data covariance $\propto \boldsymbol{\Sigma}_n^{-1}$
$\mathbf{v}, \mathbf{v}_r$	Measured voltage. $\cdot_r$: at reference time.
$\mathbf{y}$	Voltage difference data
$\mathbf{x}, \hat{\mathbf{x}}$	Image distribution. $\hat{\mathbf{x}}$: estimated.
$Z_{C,ES}$	electrode-surface contact impedance
$Z_{C,EB}$	electrode-body contact impedance

Figure 3: Block diagram of frequency-difference EIT imaging of cancerous breast tissue. A: EIT imaging plane through breast, for which, B: the frequency spectra of non-malignant (*N*) and malignant (*M*) tissue, at selected frequencies f_1, f_2 at which the spectra differ; C: reconstructed frequency-difference EIT image, illustrating typical blurring and artefacts, and, D: processed EIT image, selecting regions which exceed a threshold and are of a minimum size.

inspired air is forced to go to the upper regions, increasing the local pressure and stress. Figure 4 illustrates use of EIT to identify lung regions with low flow.

Here, the parameter of interest is the decreasing conductivity of lung tissue as it expands due to inspired air. Using continuous measurement, a time-series of EIT images can be reconstructed. From analysis of the pixel waveforms in each image, it is then possible to calculate functional parameters, such as the tidal variation (TV) — the maximum pixel change over a breath. From these parameters, functional images, such as the tidal variation image, or a thresholded image to identify low TV lung regions, can be calculated.

EIT has been proposed for numerous applications. In some cases, the technology is starting to be used clinically and extensive clinical and experimental data exists, while, in others, only a preliminary evaluation has been performed. In the rest of this section we provide an overview and references to a variety of EIT applications. In many cases, multiple references could be given; we aim to give an early or important reference.

- *Lung function* (table 2): EIT is very sensitive to the contrast between the relatively large gas volumes moving in the lungs and other chest tissues. EIT has seen the largest interest for its use in monitoring breathing, since EIT is able to non-invasively provide information on the distribution of gas within the lungs, and not only the total flows and volumes. Clinically, lung function measurement is important for patients receiving ventilatory support (invasive or non-invasive) in order to optimize the ventilation settings and to avoid possible ventilator-induced lung injury. Another useful application for EIT is lung-function testing for obstructive lung diseases, such as asthma or COPD (chronic obstructive pulmonary disease)

- *Perfusion and cardiac function* (table 3): EIT is sensitive to the movement (perfusion) of (conductive) blood through the heart and the pulmonary and systemic vasculature. Clinically, the pressures and flows of blood are relevant to patients in anaesthesia, intensive care and for sports medicine. The signal levels are lower than those from ventilation, and there are challenges to separating heart-related signals from other sources of EIT measurements.

- *Neural & brain activity* (table 4): EIT is sensitive to several phenomena of interest for medicine of the brain and neural system. Nerves change conductivity when active, and this can be imaged using EIT. Additionally, there are changes in impedance due to pathological states, such as stroke.

- *Cancerous tissue* (table 5) has different impedance
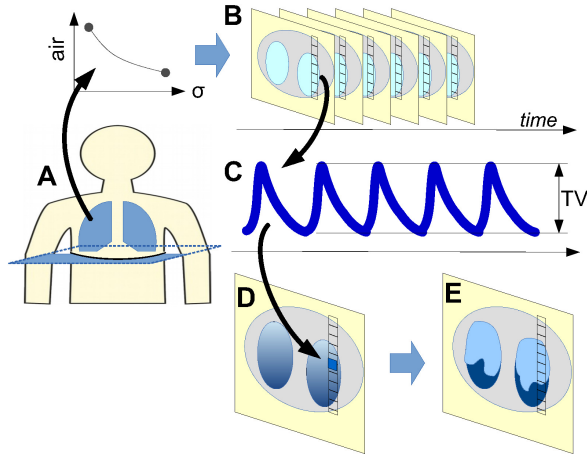
Figure 4: Block diagram of time-difference EIT imaging of lungs. A: patient breathing from which an EIT "slice" image is reconstructed; increasing air volume reduces conductivity, from which, B: time-sequence of reconstructed EIT images, and C: the time course of a single pixel from the images. From each pixel, the tidal variation (TV) is calculated and, D: a TV fEIT image is created, from which, E: a thresholded image shows pixels with low TV.

spectrum from benign tissue (61), due to changes in cancerous cell morphology, and the angiogenesis in cancerous regions. In many cases, these contrasts are larger than those available from other imaging modalities. EIT screening has been investigated for numerous types of cancer using either frequency difference or absolute image reconstruction.

- *Other* (table 6): Several other medical applications of EIT have been proposed, which do not fall into the above categories. We list several here; however, not all applications are listed.

3   Electrical Properties of Tissues

Electric fields in the body are induced by current applied through electrodes. The electric field causes ions to move through the body (measured as conductivity σ). When those ions are polarized they will also rotate to orient themselves along the field (measured as permittivity ϵ). Permittivity is treated as a function of frequency ω to give a complex-valued admittivity, $\sigma^* = \sigma + j\omega\epsilon$. Biological bodies have cell membranes and structure which can limit charge separation and trap ions at boundaries (42, 48, 73). At low frequencies, ions will travel around cell boundaries while at high frequencies those charges will move across cell boundaries at a variety of scales depending on the wavelength of the field (figure 5).

The modelling of the frequency-dependent admittivity of various biological materials is sometimes accomplished by fitting model parameters to the impedance

Table 2: EIT applications for lung function

Distribution of tidal volume
the spatial distribution of inspired air during each breath, which varies with ventilator settings (54).

Regions of overdistention, atelectasis
the fraction of lung tissue in pathological states like overdistention or atelectasis (collapse) is a useful clinical metric for patients management (51, 36).

Recruitment/derecruitment of lung tissue
recruitment of lung tissue refers to the opening of previously collapsed tissue, while derecruitment is the opposite process (45).

Regional compliance
Compliance characterizes the ease with which lung tissue accepts new volume, and can be characterized by EIT on a regional basis ($\Delta Z/\Delta P$) (38).

Respiratory system mechanics
The mechanical properties of the respiratory system can be characterized by a compliance, resistance and a time constant (their product). Characterization of such properties on a regional basis provides useful information on the state of lung tissue (79).

Opening and closing pressures
these pressures indicate the thresholds at which recruitment and derecruitment occur, and EIT is able to measure them on a regional basis (78).

Edema and extra-vascular lung water
Pulmonary edema is the accumulation of extra-vascular fluid in the lungs. It impairs gas exchange and lung function, and can occur due to left-ventricular insufficiency or lung tissue injury. EIT has shown some ability to monitor changes in the amount of lung fluid as a function of time and intervention (91).

Alarms: one-lung ventilation, pneumothorax
One important clinical requirement is the generation of alarms when dangerous ventilation conditions exist. EIT shows the potential to detect several cases of this type (72).

spectra (28). Two common models are the Debye model (39) and the Cole-Cole model (34). In general, biological tissues *in vivo*, exhibit a variable admittivity over frequency which is difficult to represent with simple models.

Specific microscopic structures, extracellular matrices (for example, bone) and tissues combine to form larger organs over which the electric field is applied. The behaviour of heterogeneous structures leads to the application of "mixing models" which represent the effective medium (70). Biological structure also leads to complex admittivity which is anisotropic. For example, admittivity will be greater in the direction of muscle fibres than across those fibres.

EIT systems typically operate at select frequencies, giving a single and largely real-valued admittivity for each measurement which is frequently approximated as a simple but frequency-dependent conductivity σ. This agrees

Table 3: EIT for perfusion and cardiac function

Regional Distribution of blood flow (86):
>The distribution of perfusion in the lungs is an important parameter and, clinically, its distribution needs to match the distribution of ventilation. Some information is available continuously from frequency-filtering of EIT data.

Ventilation-perfusion matching (84):
>The imaging of whether there is a match of the regional distribution of ventilation and perfusion is potentially a useful ability of EIT.

Contrast-based perfusion measurement (44):
>Accurate measurement of blood flow is possible with the use of a hypertonic-saline injection into the veins. The contrast can be imaged as it propagates through the right heart, lungs, left heart and into the systemic vasculature.

Cardiac output (24):
>The blood flow output of the heart is the heart rate times the stroke volume, and is an important clinical index. EIT is sensitive to blood flow and movement of the heart.

Systemic blood pressure (via pulse timing) (87):
>Blood pressure changes can be measured by EIT via the pulse transit time from the heart to the descending aorta.

Pulmonary blood pressure (via pulse timing) (77):
>Pulmonary blood pressure changes can be measured by EIT via the pulse transit time from the heart to the pulsatile signals in the lungs.

Intravascular fluid responsiveness (92):
>Fluid responsiveness is a measure of the hydration state of a patient. EIT can measure variation in stroke volume throughout the breathing cycle as an index of inadequate vascular fluid.

Table 4: EIT for neural and brain activity

Stroke (Hemorrhagic vs. Ischemic)
>The two main types of cerebral stroke need to be rapidly distinguished in order to guide emergency treatment. EIT can potentially fill this role by detecting the conductive blood present in hemorrhagic stroke (82).

Epileptic regions and foci
>EIT is sensitive to the conductivity changes in active epileptic regions, and could potentially help diagnose and monitor patients (80).

Cerebral perfusion
>Blood flow though the brain can be imaged by EIT using a conductive contrast in the blood flow (6).

Neural activation
>Neural activation changes tissue impedance by opening ion channels in nerves. These changes and the spatial and temporal pattern of activation can be used to create 4D (3D+time) of brain response to stimulation (13).

Cerebral edema
>Fluid accumulation in the brain is in important clinical concern. EIT shows potential to monitor the changes in conductive fluid (58).

Table 5: EIT to detect cancerous tissue

Breast cancer screening
>EIT has seen several studies investigating its use for screening for breast cancer (14, 32).

Prostate cancer screening
>EIT has been investigated for screening for prostate cancer (20, 53).

EIT + mammography
>The combination of EIT and mammography has been investigated. In this case the anatomical information from mammography can be used to constrain and improve EIT image reconstruction (33).

EIT + ultrasound
>The combination of EIT and ultrasound has been investigated using the compliment of information from each modality (88).

with the quasi-static approximations applied to solve the forward model's partial differential equations, as we will see in section 5.

The conductivity of tissue is strongly affected by the presence of conductive blood, either in the vasculature or, pathologically, through hemorrhage. Blood has an unusual flow-dependent conductivity; moving blood is significantly more conductive (50), and it is not clear the extent to which conductivity increases during systole are due to increases in regional blood volumes or conductivity increases.

Errors in the measurement of tissue admittivity can be introduced by lead inductance and electrode polarization. A voltage measurement taken on the current driving electrodes (2-electrode measurements) can be compared to measurements on nearby electrodes (different electrodes used for current drive and voltage measurement, as a 4-electrode measurement) to evaluate these errors. Irrespective of these controls, tissue properties change over time as the skin sweats, hydration levels change or movement occurs, which represent confounding factors in evaluating time-series measurements. Tissue is a biological sample, so excising material to take measurements changes the properties of the tissue. These issues lead to a range of low frequency conductivity values being reported for many types of tissue (48). In many cases, physiological changes result in changes in admittivity which can be isolated from these error sources to indicate changes of clinical interest (section 2).

4 EIT Hardware

A typical EIT system consists of a digital controller, analog-to-digital (A/D) and digital-to-analog (D/A), current sources, differential voltage sensors, a mechanism to switch between electrodes, wiring between the system and the electrodes, and the electrodes themselves, sometimes embedded in a belt or other structure. A typical

Table 6: EIT for other applications

Gastric and Intestinal motility
> The rate and flow of food in the stomach and intestines has useful diagnostic value for many conditions. EIT is sensitive to conductivity-contrasting food and fluids (69).

Pharyngeal transit times
> EIT can be used to measure the rate at which fluid passes through the pharynx (69).

Bladder volume and emptying
> Conductive urine creates a contrast which can be identified by EIT. There are several uses of this information, such as monitoring the level of bladder filling (for sedated patients), and the rate of bladder emptying (63).

Peripheral Edema
> Fluid accumulation in peripheral edema creates a contrast which can be identified in EIT images, and monitoring of the accumulation and dissipation is diagnostically useful (1, 74).

Hemorrhage and blood accumulation
> The accumulation of conductive blood in hemorrhagic tissue can be identified in EIT images, and monitoring of the level of hemorrhage is clinically useful (83).
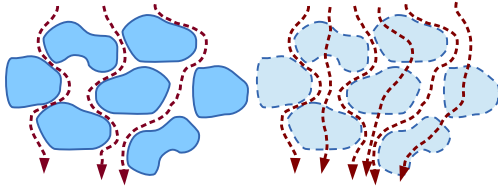
Figure 5: Low frequency (left) and high frequency (right) current flows through a heterogeneous biological medium along different paths depending on the wave length of the electric field in relation to the cell size at a variety of scales according to macroscopic, cellular, ionic and molecular structure.

digital controller consists of an field programmable gate array (FPGA) and microcontroller which collaborate to perform calculations, store data, and transfer the results to a host system. The FPGA controls the current sources and measurement functions using A/D and D/A converters to drive current and measure voltage. Demodulation and sine wave generation are commonly part of the digital infrastructure in modern systems.

Low amplitude sinusoidal current (milliamps) is driven through the body at a pair of electrodes by matched current sources (at $180°$ phase) at a relatively low fixed frequency, typically between $10\,\mathrm{kHz}$ to $250\,\mathrm{kHz}$, although some systems operate below $1\,\mathrm{kHz}$ to measure specific frequencies of interest. Voltage measurements are made between pairs of electrodes or between electrodes and a reference (ground) electrode. These "difference" voltage measurements are in the millivolt to microvolt range, and are subject to many sources of measurement interference.

New electrodes are selected for both current and voltage by multiplexing between many electrodes, which can introduce switching transients. Typical systems have sixteen to sixty-four electrodes.

The complete sequence of electrode pairs used for stimulus and measurement provides a "frame" of data. The measurements making up a frame are repeated to produce a time series. Figure 6 illustrates a common sequence of current stimulation and voltage measurements as part of a data frame, using two stimulation and measurement patterns. The earliest EIT systems were based on adjacent ("skip" 0) stimulation and measurement (25), while more recent systems often use a larger "skip" value to increase the sensitivity at depth. For an N_E electrodes system using pair-drive and measurement, there are $\frac{1}{2}N_E(N_E - 3)$ measurements to be made, when reciprocal measurements and measurements on driven electrodes (2-electrode measurements) are avoided (59). Modern EIT systems can achieve high frame rates (commercial systems provide 50 frames/s) which is enough to detect most physiological activity. However, system noise performance decreases with increasing frame rates, so it is recommended to measure at a rate consistent with the physiology of interest. The system can be accelerated by adding more current sources and differential measurement devices at the cost of additional challenges in achieving and maintaining calibration between channels.

In principle, EIT hardware should not be difficult to implement: it operates at low frequency and low current. Currents are limited by safety concerns which have been codified in the standards for medical devices (65), limiting the maximum current to $10\,\mathrm{mA}$ at frequencies of $100\,\mathrm{kHz}$ and above (60). Challenges arise from low noise requirements, wide dynamic range, and the dramatic decrease in Common Mode Rejection Ratio (CMRR) at typical EIT operating frequencies when compared to DC measurements; most operational amplifiers have CMRR performance that drops dramatically around $10\,\mathrm{kHz}$. The wide dynamic range and common mode voltages of the measurements results from taking these measurements at a variety of locations and electrode separations on the body. Voltage measurement electrodes adjacent to current electrodes will have the largest voltage difference, while electrodes far from the current carrying electrodes may have very small differential voltages.

Two types of electrodes are available: polarizable and non-polarizable electrodes, which are distinguished by their behaviour at the electrode-electrolyte interface where an "electrical double layer" of charge forms. For example, stainless steel and platinum electrodes are polarizable, while Ag/AgCl electrodes are not. Ideal polarizable electrodes have an interface that behaves as a capacitor, while ideal non-polarizable electrodes behave resistively. In either case, movement of the electrode sep-
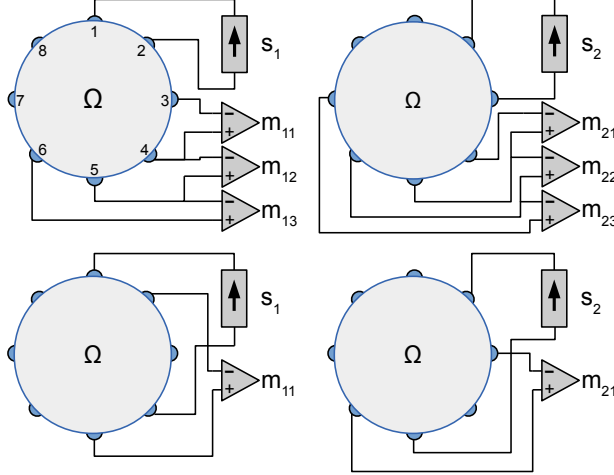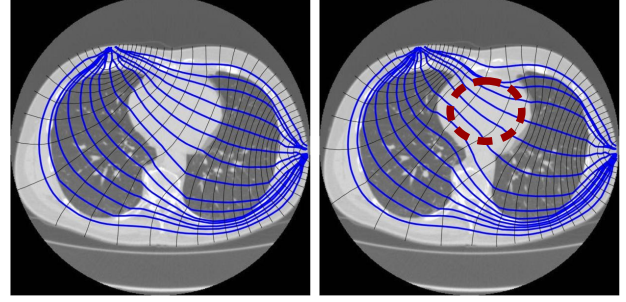
Figure 6: Stimulation and measurement patterns using an adjacent pattern (*top row*) and a "skip 2" pattern (*bottom row*) for an eight electrode EIT system, in which measurements are not made on driven electrodes. The first column shows the measurements $m_{11} \ldots m_{1n}$ due to the first stimulation s_1, and the second column shows the measurements $m_{21} \ldots m_{2n}$ due to the second stimulation.

Figure 7: Illustration of the propagation of current in a body. In each image, a FEM of a volumetric model of the thorax is used to simulate the propagation of electric current from a pair of surface electrodes with the indicated current source. Blue lines show current streamlines while the black lines are isopotential surfaces. From the left to right, an increase of conductivity in the heart (dotted red lines) is simulated.

arates the electrical double layer introducing motion artefacts into the time-series measurements which resolve as the double layer reforms. Electrodes are also of a particular size and can provide a preferential current path over the skin surface, even when inactive, if the electrode's internal conductivity is lower than the body (see figure 8), as is typically the case. The choice between the two types of electrode is application specific: non-polarizable electrodes typically use an aqueous gel which dries over time changing contact impedances, while polarizable electrodes can be more susceptible to motion artefacts.

5 Forward Problem

The physics of current propagation in the body are determined by Maxwell's equations. The term "forward problem" has been used to describe the calculation of the current and voltage distribution in the body and then sensitivity of an EIT system as a function of position. To illustrate, figure 7 shows current streamlines in a finite element model of the thorax. Current is applied through a pair of electrodes. As the conductivity of the heart increases due to the presence of conductive blood during diastole, the pattern of current streamlines and isopotential lines changes. The moving isopotential lines indicate the changes in measured voltage on other body-surface electrodes.

At the relatively low frequencies used in EIT, it can be approximated as an electrostatic system, which is mathematically equivalent to the heat equation. In this limit, electric current propagates diffusively and "spreads out" away from electrodes. This diffusive nature of the physics of low frequency electric current has two main consequences for EIT. First, EIT is extremely sensitive to any changes at or near the electrodes. Reconstructed images can show large artefacts when electrodes move, dry out (changing contact quality) or are incorrectly modelled in terms of shape and size. Next, EIT is much less sensitive further from the electrodes, which is often the region of interest in the interior of the body. The large ratio in sensitivity between the high- and low-sensitivity regions indicates that EIT image reconstruction is "ill conditioned."

To derive the equations of the EIT forward problem, take a body Ω in three-dimensional space with spatial variable $r = (x, y, z)$. We assume the body has isotropic conductivity $\sigma(r)$, permittivity $\epsilon(r)$, and permeability $\mu(r)$, and these properties are potentially inhomogeneous throughout the body.

EIT systems generally apply fixed-frequency currents and voltages to the body. For an angular frequency ω, time-varying properties may be replaced with phasor representations, and the time-derivatives with $j\omega$. A time-harmonic current density $\mathrm{J}(r, t) = J(r)e^{-j\omega t}$ is applied to the surface $\partial\Omega$, and this results, after some settling time, in an electric field $\mathrm{E}(r, t) = E(r)e^{-j\omega t}$ and magnetic field $\mathrm{H}(r, t) = H(r)e^{-j\omega t}$ in the body. Using Ohm's law, $J = \sigma E$, Maxwell's equations give us,

$$\begin{aligned} \nabla \times E &= j\omega\mu H \\ \nabla \times H &= (\sigma + j\omega\epsilon)E = \sigma^* E \end{aligned} \tag{1}$$

where ∇ is the Del operator $(\frac{\partial}{\partial x}, \frac{\partial}{\partial y}, \frac{\partial}{\partial z})$. We define the complex conductivity or admittivity $\sigma^* = \sigma + j\omega\epsilon$, and use (eqn 1) and the identity, $\nabla \cdot (\nabla \times X) = 0$,

$$\nabla \cdot (\nabla \times H) = \nabla \cdot \sigma^* E = 0, \tag{2}$$

When permeability and frequency are sufficiently small, we can make the approximation, $\nabla \times E = 0$, in which case the electric field $E = -\nabla\phi$, is uniquely determined by a scalar electric potential, ϕ. This "quasistatic" approximation is valid when the geometric scales of interest are much smaller than the electromagnetic wavelength $(\omega\sqrt{\mu\epsilon})^{-1}$ (62). For example, in tissue, $\mu \approx 1$ and $\epsilon \leq 10 \times \epsilon_0$, so for $f = 100\,\text{kHz}$, $(2\pi f\sqrt{\mu\epsilon})^{-1} \approx 3\,\text{km}$.

These equations define the Laplace (or Poisson's) equation which controls the EIT forward problem

$$\nabla \cdot (\sigma^* \nabla\phi) = 0, \tag{3}$$

and is subject to boundary conditions which specify the normal current (Neumann boundary conditions) or potential (Dirichlet boundary conditions) at the electrodes. Additionally, a reference voltage must be specified at some point, either at a ground electrode or elsewhere on the body.

At an electrode, electrical current distributes through the electrode material and flows into the body, changing from being carried by electrons to ions at the electrode-body interface. Especially at low frequency (DC to 100 Hz), the interface is dominated by complicated electrochemical processes; however, for most EIT systems the frequencies used are such that the electrode-skin impedance is fairly low, especially when the skin is not dry or a suitable electrode gel is used.

As mentioned, EIT current density, and therefore sensitivity, is highest at the electrodes and decreases elsewhere. This means that accurate electrode models are important for EIT accuracy. Most electrodes are fabricated from conductive material, and thus offer an "easier" current path than the bulk material. Figure 8 shows the propagation of current near measurement and drive electrodes, and illustrates that most current flows near the edges of electrodes

Several models of electrodes have been used (30), including those which assume uniform current magnitude across each electrode (the "continuum" and "gap" models). If the electrode material is much more conductive than the body, a "shunt" model creates a constant voltage across the electrode. Most recent work uses a "complete electrode model" (CEM), which accounts for the electrical properties of the electrode material, $Z_{C,ES}$ (31). Here we distinguish between two parameters of the electrodes which have both been called the "contact impedance". The electrode-body contact impedance, $Z_{C,EB}$ is the load through which the EIT hardware must send current, while the electrode-surface contact impedance, $Z_{C,ES}$, characterizes the electrode material.

Calculation of potential ϕ throughout the body requires the solution of (eqn 3) for the boundary conditions given by the electrode models and each of N_C applied pattern of current to the N_E electrodes. No analytic solutions of
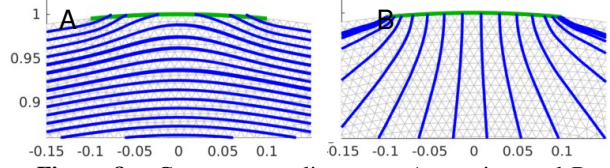
Figure 8: Current streamlines near A: passive, and B: drive electrodes, using 2D FEM with $Z_{C,EB} = 0.01$.

this equation exist for arbitrary geometries, so it must instead be approximated numerically. The most common numerical technique is the finite element method (FEM), which is preferred because it allows refinement in regions of high current, such as near the electrodes (52). In most cases, EIT researchers have used the most simple models, first-order tetrahedral elements. The body is discretized into N_F finite elements, and the complex admittivity in each is represented by a vector $\boldsymbol{\sigma}_F \in \mathbb{C}^{N_F}$. For notation, the vectors representing the state of the system or a frame of measurements at a given time are in bold font and consist of complex values of the given size. The FEM calculates a voltage distribution throughout the body for each admittivity distribution, $\boldsymbol{\sigma}_F$, and applied electrode current distribution, $\mathbf{I}$. From the body voltage distribution, a vector of voltages at electrodes is extracted. By successively calculating the electrode voltages for each applied current pattern, a frame, $\mathbf{v} \in \mathbb{C}^{N_m}$, of EIT data is simulated. Many FEM software packages allow vectorized solution of the voltages for multiple current patterns. The maximum number of independent measurements possible on N_E electrodes is $\frac{1}{2}N_E(N_E-1)$, due to reciprocity (i.e. the sensitivity is unchanged if drive and measurements are interchanged) (66). If one further restricts the measurements to be away from the stimulus electrodes, preventing 2-electrode measurements which are more sensitive to contact impedance and electrode movement, this removes an additional N measurements leading to the oft quoted $\frac{1}{2}N_E(N_E - 3)$. Typically, a data frame is considered to represent the impedivity of the body at an instant; however the measurements are slightly asynchronous for serial, multiplexed EIT systems.

Here, we introduce a notation to consistently describe the forward computations for absolute, frequency difference and time difference EIT. We define the "measured data", $\mathbf{y} = \mathbf{v}$ for absolute EIT, and $\mathbf{y} = \mathbf{v} - \mathbf{v}_r$, for difference EIT, as it reconstructs the change in admittivity between the measurement of interest, $\mathbf{v}$, and $\mathbf{v}_r$. Two variants of difference EIT are also used: normalized difference EIT uses $\mathbf{y} = (\mathbf{v} - \mathbf{v}_r)./\mathbf{v}_r$, where $./$ is element-wise division; and frequency difference EIT, where the measurements, $\mathbf{v}_r$ must be scaled such that $\mathbf{y} = \mathbf{v} - k\mathbf{v}_r$ (85). The measured data, $\mathbf{y}$, can have complex values corresponding to the in- and out of-phase components, although at low frequencies (below a few hundred kHz) the

8

conductive (in-phase) component dominates.

The image parameters, $\mathbf{x}$, are defined similarly to the "measured data". For absolute EIT, the reconstructed image of interest is the admittivity, $\mathbf{x} = \boldsymbol{\sigma}$, while for difference EIT, the image of interest is the admittivity change, $\mathbf{x} = \boldsymbol{\sigma} - \boldsymbol{\sigma}_r$ with respect to its value at a reference instant. It is also common to parameterize the image differently to the forward FEM, such that we calculate $\boldsymbol{\sigma}_F = \mathbf{M}\boldsymbol{\sigma}$, where $\mathbf{M}_{i,j}$ is a coarse-to-fine projection, representing the volume fraction of FEM element j in each image element i. This different parameterization is useful when using a refined mesh in the vicinity of electrodes, which helps an accurate forward calculation, but is not desired in the images. The FEM-based forward calculation is represented

$$\mathbf{y} = F(\mathbf{x})|_{\boldsymbol{\sigma}=\boldsymbol{\sigma}_r}. \qquad (4)$$

For difference EIT, $\mathbf{v}_r$ is calculated at an assumed reference conductivity, $\boldsymbol{\sigma}_r$.

For an imaging system, it is important to characterize the sensitivity in terms of the expected change in measured parameters for a given change in parameters of interest. The sensitivity serves to characterize the ability of a given EIT configuration (body shape, electrode positions, stimulation and measurement pattern) to detect contrasts of interest. The sensitivity is also an important part of the image reconstruction process. Sensitivity is represented by a Jacobian, $\mathbf{J}$, or sensitivity matrix. Each component $[\mathbf{J}]_{i,j}$ represents the sensitivity of measured data, i, to image parameter j.

$$\mathbf{J}_{i,j} = \left. \frac{\partial}{\partial \boldsymbol{\sigma}_j} F(\mathbf{x})_i \right|_{\boldsymbol{\sigma}=\boldsymbol{\sigma}_r}. \qquad (5)$$

The matrix, $\mathbf{J}$, may be calculated by direct differentiation of the FEM system matrix formulation (94), and by using adjoint field methods (76). Direct differentiation requires a custom FEM solver, while the adjoint field methods can accept the output of packaged FEM algorithms, by integrating over the inner product of the electric fields produced by stimulation and measurement patterns in each image element. Efficient implementation of either methods results in the same algorithm (10). It is sometimes useful to approximate $\mathbf{J}$ using small changes in each image region to calculate a "perturbation Jacobian" (94). Columns of $\mathbf{J}$ represent the change in measurements, $\partial \mathbf{v}$, due to a conductivity contrast in the corresponding FEM element, while each row represents the relative contribution to each FEM element from the corresponding measurement. Figure 9 illustrates the sensitivity of EIT for several patterns of current injection and voltage measurement.

The sensitivity of EIT in three dimensions presents a complicated structure, even for a traditional, single plane of electrode placements. Figure 9 shows a "lens-shaped"
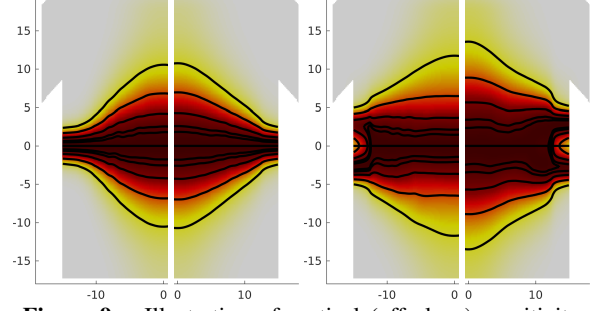
Figure 9: Illustration of vertical (off-plane) sensitivity of EIT for one (*left*, with 32 electrodes) and two (*right*, with 2×16 electrodes) electrode planes. Data are simulated with a homogeneous elliptic model, and sensitivity shown on frontal plane through the centre. Sensitivity in each vertical row is normalized to the maximum value. Contours at 90%, 75%, 50%, and 25% are shown. For each figure, the left image uses an adjacent stimulation and measurement pattern, while the right shows "skip=4".

sensitive region, in which EIT is sensitive to off-plane conductivity contrasts.
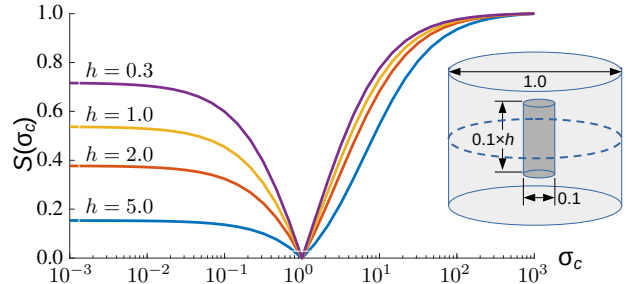
Figure 10: The relative EIT sensitivity, $S(\sigma_c)$ as a function of the shape and conductivity of a ROI. The stimulation configuration (subfigure at right) has 16 electrodes in a central plane (dotted), and has a contrasting cylindrical ROI with a height/diameter, h, and conductivity σ_c while elsewhere $\sigma = 1$. The graph shows the normalized EIT signal, $S(\sigma_c)$, as a function of σ_c for four values of h.

6 Image Reconstruction

Image reconstruction is the term used in the inverse problems and tomographic imaging literature to describe the calculation of an image from projection data. Image reconstruction is typically a challenging problem as it is ill-conditioned and often ill-posed. The ill-conditioning stems from the large difference in sensitivity between regions (the electrodes and the body centre in EIT). EIT is also ill-posed because it is not possible to estimate a large number of image parameters from the limited number of measurements in each data frame.

Image reconstruction is formulated as an inverse problem which calculates an estimate, $\hat{\mathbf{x}}$, of the distribution of

internal properties, $\mathbf{x}$, which best explains the measurements, $\mathbf{y}$. A simplified schema for image reconstruction is shown in figure 11, which illustrates the process by which model parameters are iteratively adjusted to fit the measurements (and "prior" image constraints). The reconstructed image is the model after iterations are stopped upon convergence.
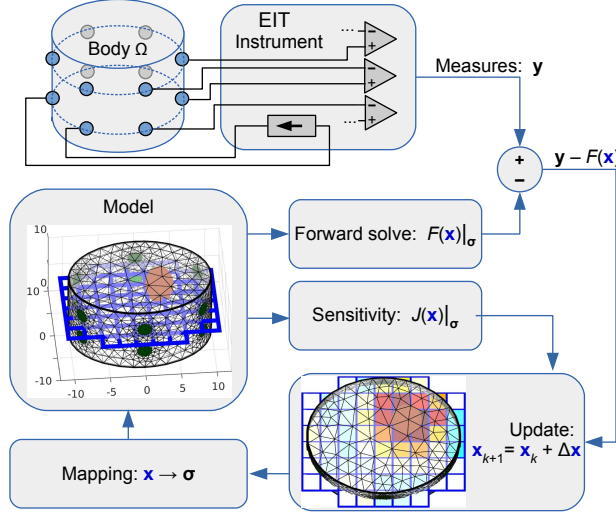
Figure 11: Schema for image reconstruction based on model fitting. EIT data, $\mathbf{y}$, are measured with an instrument from body Ω. Iteratively, a model $\mathbf{x}_k$ is improved by updates, $\Delta\mathbf{x}$, calculated from the mismatch between the current forward estimate and sensitivity, and a prior model. The mapping between image parameters, $\mathbf{x}$, of a planar slice, and the 3D FEM-based model are illustrated.

Image reconstruction in EIT has traditionally been divided into algorithms for difference EIT (section 6.1) and absolute EIT (section 6.2). Difference EIT is more stable and can be feasibly reconstructed with linear techniques, while absolute EIT is a more difficult problem and requires advanced methods. In contrast to geophysical ERT, in which absolute reconstructions are common, experimental and clinical EIT has almost exclusively used difference measurements and algorithms. For successful absolute reconstructions, it is necessary for the model to be accurate in terms of body geometry and electrode positions, shapes and contact impedances, as well as hardware and electronics imperfections. For difference EIT, shape and electronics modelling inaccuracies are less significant, as long as they remain the same between the difference measurements.

6.1 Difference EIT

The most common approach to difference EIT image reconstruction uses a regularized framework to minimize the norm

$$\|\mathbf{y} - F(\hat{\mathbf{x}})\|_{\mathbf{W}}^2 + \lambda^2 \|\hat{\mathbf{x}} - \mathbf{x}_0\|_{\mathbf{Q}}^2, \qquad (6)$$

where the first term $\mathbf{y} - F(\hat{\mathbf{x}})$ is the "data mismatch" between the measured data and their estimate via the forward model. $\mathbf{W}$ is a data weighting matrix, and represents the inverse covariance of measurements. The 2-norm represented as $\|\mathbf{a}\|_{\mathbf{A}}^2 = \mathbf{a}^T \mathbf{A}\mathbf{a}$, for positive definite $\mathbf{A}$. The second term is the mismatch between the reconstruction estimate, $\hat{\mathbf{x}}$, and an *a priori* estimate of its value, $\mathbf{x}_0$. $\mathbf{Q}$ is the "regularization matrix". The relative weighting between the data and prior mismatch terms is controlled by a hyperparameter, λ. When λ is large, solutions tend to be smooth and more similar to the prior; while, for small λ, solutions have higher spatial resolution, but are noisier and less well conditioned.

The norm (eqn 6) may be best understood from a Bayesian maximum a posteriori scheme as follows

$$p(\mathbf{x}|\mathbf{y}) = \frac{p(\mathbf{y}|\mathbf{x})p(\mathbf{x})}{p(\mathbf{y})} \propto p(\mathbf{y}|\mathbf{x})p(\mathbf{x}) \qquad (7)$$

where $p(\mathbf{x}|\mathbf{y})$ is the reconstructed quantity of interest, and maybe interpreted as the likelihood of the "correct" image being $\mathbf{x}$ given measured data $\mathbf{y}$. Here, $p(\mathbf{x})$ is the "a priori" distribution of possible image parameters, and $p(\mathbf{y})$ the distribution of measured data, which is not needed, since the goal is to find the maximum $p(\cdot)$.

The likelihood of measurements $\mathbf{y}$ given image parameters $\mathbf{x}$ is determined by the forward model and the distribution of likely noise from the hardware. Modelling $\mathbf{y} = F(\mathbf{x}) + \nu$, with noise, ν with a Gaussian distribution, $\nu \sim \mathcal{N}(0, \Sigma_n)$, we have

$$p(\mathbf{y}|\mathbf{x}) = \exp\left(-\|\mathbf{y} - F(\mathbf{x})\|_{\Sigma_n^{-1}}^2\right). \qquad (8)$$

We represent the inverse covariance of the data weighting matrix, as a product, $\Sigma_n^{-1} = \sigma_n^2 \mathbf{W}$, of a scalar noise power, σ_n^2 and a structural matrix $\mathbf{W}$, which represents the relationship between noise on measurement channels. In most cases, $\mathbf{W}$ is set to be the identity matrix, corresponding to a model of independent and equal measurement channels; however, given a knowledge of the reliability of each measurement channel, $\mathbf{W}$ can be used to represent this reliability during reconstruction (68).

In an inverse problem, it is not sufficient to use only (eqn 8) to reconstruct images; the very low sensitivity of measurements to some image parameters (such as voxels far from the boundary) means that small noise values in the data result in large noise in the reconstructed images. Image reconstruction thus requires regularization to impose additional constraints (or penalties) on the images. We review below a number of regularized schemes.

In our opinion, the most natural way to understand regularization is through the Bayesian parameter $p(\mathbf{x})$. This

parameter is called the *prior* model, or the *a priori* information, since it describes information about possible images, $\mathbf{x}$, before any measurements, $\mathbf{y}$, are made.

Many *prior* models are used; the simplest computationally is a Gaussian distribution $\sim \mathcal{N}(\mathbf{x}_0, \Sigma_x)$, we have

$$p(\mathbf{x}) = \exp\left(-\|\mathbf{x} - \mathbf{x}_0\|^2_{\Sigma_x^{-1}}\right). \tag{9}$$

where Σ_x models the expected amplitude and spatial covariance of image parameters. For difference EIT, $\mathbf{x}_0 = 0$, since increases and decreases are equally likely. We represent the inverse covariance as a product $\Sigma_x^{-1} = \sigma_x^2 \mathbf{Q}$, of a scalar image power, σ_x^2 and a structural matrix $\mathbf{Q}$, which is discussed below. The hyperparameter, $\lambda = \frac{\sigma_x}{\sigma_n}$ represents a ratio of the "strength" of the regularization and noise constraints.

From (eqn 7), we have

$$p(\mathbf{x}|\mathbf{y}) \propto p(\mathbf{y}|\mathbf{x})p(\mathbf{x})$$
$$= \exp\left(-\|\mathbf{x} - \mathbf{x}_0\|^2_{\Sigma_x^{-1}}\right)\exp\left(-\|\mathbf{y} - F(\mathbf{x})\|^2_{\Sigma_n^{-1}}\right)$$
$$\propto \exp\left(-(\|\mathbf{x} - \mathbf{x}_0\|^2_{\mathbf{W}} + \lambda^2\|\mathbf{y} - F(\mathbf{x})\|^2_{\mathbf{Q}})\right).$$

The MAP (or Maximum a posteriori) solution is the value $\hat{\mathbf{x}}$ which maximizes $p(\mathbf{x}|\mathbf{y})$. It is *a posteriori* in the sense that it is our estimate of the image taking into account (i.e. *after*) the measurements. Thus,

$$\hat{\mathbf{x}} = \underset{\mathbf{x}}{\operatorname{argmax}}\ e^{-\left(\|\mathbf{y} - F(\mathbf{x})\|^2_{\mathbf{W}} + \lambda^2\|\mathbf{x} - \mathbf{x}_0\|^2_{\mathbf{Q}}\right)}$$
$$= \underset{\mathbf{x}}{\operatorname{argmin}}\ \|\mathbf{y} - F(\mathbf{x})\|^2_{\mathbf{W}} + \lambda^2\|\mathbf{x} - \mathbf{x}_0\|^2_{\mathbf{Q}}. \tag{10}$$

The MAP estimate is when then exponential is maximized, and the norm has a minimum.

Starting from an estimate $\mathbf{x}_0$, the Gauss-Newton scheme allows an iterative approximation, by, at each step calculating an update $\Delta\mathbf{x}_k$, such that

$$\mathbf{x}_{k+1} = \mathbf{x}_k + \Delta\mathbf{x}_k, \tag{11}$$

where at each step, the update would solve the linearized problem, around the current estimate $\mathbf{x}_k$, using Jacobian, $\mathbf{J}_k = \frac{\partial}{\partial\mathbf{x}}F(\mathbf{x})|_{\mathbf{x}_k}$.

$$\Delta\mathbf{x}_k = \left(\mathbf{J}_k^t\mathbf{W}\mathbf{J}_k + \lambda^2\mathbf{Q}\right)^{-1}\left(\mathbf{J}_k^t\mathbf{W}(\mathbf{y} - F(\mathbf{x}_k)\ + \right.$$
$$\left. \lambda^2\mathbf{Q}(\mathbf{x}_0 - \mathbf{x}_k)\right)$$

In most cases, a one-step regularized difference EIT solution is used (29), in which case (eqn 12) reduces to a matrix multiplication, $\hat{\mathbf{x}} = \mathbf{R}\mathbf{y}$, with a reconstruction matrix $\mathbf{R}$, where

$$\mathbf{R} = \left(\mathbf{J}^t\mathbf{W}\mathbf{J} + \lambda^2\mathbf{Q}\right)^{-1}\mathbf{J}^t\mathbf{W} \tag{12}$$

since $\mathbf{x}_0$ and $F(\mathbf{x}_0)$ are zero for difference EIT. In some cases the matrix to be inverted in (eqn 12) is large, and the

equivalent expression in the "Wiener filter" form may be used (4):

$$\mathbf{R} = \mathbf{Q}^{-1}\mathbf{J}^t\left(\mathbf{J}\mathbf{Q}^{-1}\mathbf{J}^t + \lambda^2\mathbf{W}^{-1}\right)^{-1} \tag{13}$$

While the most commonly used image reconstruction algorithms use Gaussian probability models for image (eqn 9) and noise (eqn 8) parameters, there are advantages to the use of other approaches. Using a 1-norm instead of a 2-norm in (eqn 9) is called "total variation" (TV), and produces images in which edges are preserved and not blurred (21) Using a 1-norm instead of a 2-norm in (eqn 8) produces an algorithm which is less sensitive to measurement outliers, and has been called "robust error norms" (22).

6.1.1 Regularization parameters

The behaviour of image reconstruction is controlled by the selection of the regularization matrix $\mathbf{Q}$ and the hyperparameter, λ.

Figure 12 illustrates the effect of λ, which controls the amount of regularization. As λ decreases, the image more accurately reflects the simulation, but also becomes more sensitive to noise. This "noise-resolution" trade-off is typically the most important parameter choice for an EIT configuration. Its value should be chosen to be the minimum (best resolution) which is still able to provide relatively noise-free images. A number of strategies have been used in the EIT literature to select an appropriate hyperparameter value, including the : L-curve (55), Noise Figure (2), and Image SNR (23).
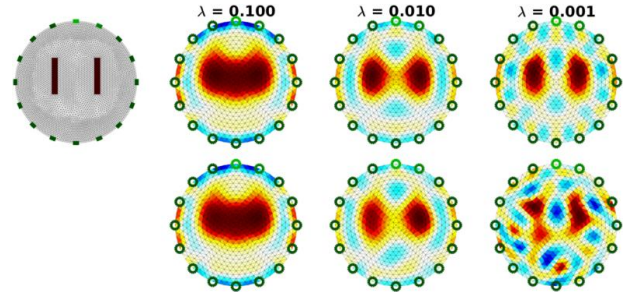
Figure 12: Reconstructed images of a 2D simulation phantom (*top left*), for various values of the hyperparameter, λ: *Top:* simulated data with no noise *Bottom:* simulated data with added Gaussian noise.

The regularization matrix $\mathbf{Q}$ imposes a structural penalty onto image elements. In the simplest case, $\mathbf{Q}$ is diagonal and imposes a penalty on image amplitude, favouring low-amplitude reconstructions; this is the case for a Tikhonov or a diagonal matrix (29). Next a matrix with off-diagonal elements can impose a spatial high-pass filter to penalize non-smooth components in the image, such as for a Laplace spatial filter (76). Another approach

is to impose regularization in a transformed space, such as the singular value decomposition (19). The amount of regularization is chosen by truncating the singular values at a chosen level. Example images are shown in figure 13, along with an edge-preserving reconstruction using total variation (22).
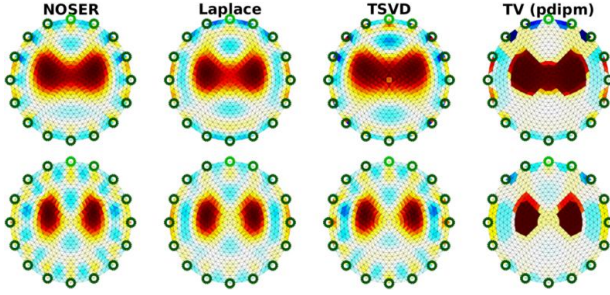
Figure 13: Reconstructed images of a 2D simulation phantom (figure 12) for various values of the structural prior, **Q**, in each column. A different value of the hyperparameter, λ, was used in each row.

6.2 Absolute EIT

Difference EIT is used to determine the change in conductivity between two frames of measurements. Absolute EIT, by contrast, determines the absolute value of the conductivity from a single frame of measurements.

For an absolute solution, an initial estimate of the solution σ_0 is calculated by fitting a homogeneous (or some low-dimensional) conductivity model to the measurements. Next, in a loop, the same principle operation as difference EIT is computed to find a single-step Gauss-Newton update $\Delta\mathbf{x}_k$, with regularization, measurement covariance, prior, and a Jacobian calculated at the current conductivity estimate. A scaling parameter ($0<\alpha<1$) for this update is determined using a line search and by solving the forward problem at $\mathbf{x}_{k+1} = \mathbf{x}_k + \alpha\Delta\mathbf{x}_k$ then evaluating the data misfit and prior penalty terms to find the minima. This process is repeated until either an iteration limit is exceeded, a tolerance is achieved for the penalty function, or the solution fails to progress. This iterative procedure is illustrated in figure 11.

Absolute EIT is more common in geophysics settings where the ability to measure before and after a change can be unusual for many applications. In these geophysics applications, it is also common to parameterize over log conductivity to address the wide range of conductivities that are encountered. Measurements are commonly normalized by dividing the measurements calculated on a forward simulation of the model with a homogeneous 1 S/m conductivity, which are called "apparent resistivity" in geophysics and "measurement normalization" in the biomedical communities. The re-scaling of measurements serves to re-weight the measurement misfit function so that small amplitude measurements will carry equal weight. The measurement re-scaling also impacts estimates of measurement noise, which should be similarly scaled, because the apparent signal-to-noise ratio has changed. Scaling conductivity and measurements has a significant effect on appropriate values for regularization parameters which will sometimes change by orders of magnitude.

Absolute EIT is typically more challenging than difference EIT because many sources of error are no longer cancelled and must be either carefully measured and controlled or incorporated into the reconstruction. The primary cause of reconstruction artefacts tends to be geometric mismatches between the reconstruction model and the measured surface, particularly the electrode locations. Model induced artefacts due to model-measurement mismatch can be particularly misleading because they will remain consistent when reconstruction parameters are varied and over many repeated measurements at the same location.

Other important error sources include electrode movement, electrode contact impedance, non-ideal analog circuits, and non-ideal wiring. Errors can be addressed through calibration of the EIT systems, careful equipment installation (electrode layout and contact), noting deviations from planed acquisitions, and measuring actual installed locations to very high resolution.

7 Image Analysis

After reconstruction of EIT images, the images are analysed to determine parameters relevant for the physiological application of interest. A rich literature of "functional" EIT (or fEIT) parameters has developed for analysis of time-sequences of EIT images. Techniques for fEIT analysis are subdivided by Frerichs *et al.* (47) into "functional EIT images" and "EIT measures".

Figure 14 illustrates the calculation of a "tidal variation" fEIT image and the measure of "centre of ventilation" calculated from this fEIT image. The fEIT image is based on an analysis of each pixel (or voxel) waveform and a mathematical operation is performed on it. For tidal variation, the minimum-maximum range is calculated. After calculation of this value for each pixel an fEIT image is created with the values. From the fEIT image, an EIT measure can be calculated. The centre of ventilation is the coordinates of the centre of mass of the tidal ventilation fEIT image.

Various types of fEIT images have been defined as illustrated in figure 15. Two basic categorizations are between measures which can be conducted routinely, and examination-specific measures, which require specific in-
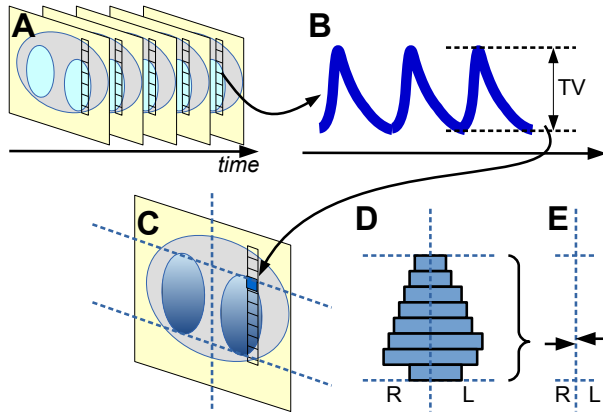
Figure 14: Illustration of calculation of functional EIT images and measures (adapted from (47)) (A) EIT image sequence, from which (B) waveforms are analysed to calculate a tidal variation (TV) parameter, from which fEIT images (C) are generated. In (D), a horizontal histogram of breathing in "slices" of the left and right lung is calculated, from which the centre of gravity (E) in the left and right lung are determined.

terventions with patients.

- *Distribution of Ventilation*: EIT measures of ventilation are determined by the tidal (within-breath) variations of the EIT pixels. These have been measured using the signal standard deviation (which was appropriate in early, low frame-rate systems, but is no longer recommended) and by the tidal variation measure shown in figure 15A.

- *Distribution of other lung volumes*: EIT allows measurement of the distribution of other physiologically-relevant volumes, such as forced vital capacity (FVC) and forced expiratory volume in 1 second (FEV_1).

- *Distribution of ratios of lung volumes or flows*, such as the ratio of FEV_1/FVC in each image pixel.

- *Distribution of Aeration change*: The change in aeration is the volume-difference in the lungs between two time points due to an intervention or physiological activity. Typically, this is measured as a change in end-expiratory lung volume ΔEELV, shown in figure 15C.

- *Frequency analysis of impedance changes*: Frequency analysis of impedance changes allows separation of breathing- and heart-related effects. If no external timing measures are available, a band-pass filtered fEIT signal can separate a Cardiac-frequency (or Pulsatility) fEIT images from the (typically much larger) Ventilation signal. While these images are useful, it is worth pointing out that they are subject

to artefacts if the heart rate changes on a beat-to-beat basis, or if harmonics of the ventilation signal overlap with the heart rate. Furthermore, the cardiac-frequency EIT signal cannot be considered a direct measure of blood flow (perfusion) since the pulsatile component of the signal is affected by many other physiological functions (11).

- *Respiratory system mechanics (non-linear compliance)*: The compliance is a non-linear function of lung volume, and is low at both low and high lung volumes due to alveolar collapse (atelectasis) or overdistention, respectively. EIT-based measures of respiratory system properties seek to characterize these aspects of the mechanical properties. First, the non-linearities in compliance have been characterized by: fEIT of landmark pressure points, such as the lower and upper inflection point pressures, (figure 15E) or fEIT of opening / closing pressures.

- *Respiratory system mechanics (time constants)*: The mechanical properties of lung tissue is typically characterized by parameters of compliance ($C = \frac{L}{kPa}$) and resistance ($R = \frac{kPa \cdot s}{L}$). EIT-derived measures of volume are mostly proportional to the dynamic compliance, but yield no information on R. Increases in tissue resistance reflects narrowing of airways and changes in parenchyma. The time constant $\tau = RC$ of tissue introduces a delay in the ventilation signal, which results in a change of phase in the regional EIT signal. The resistance and τ values have been characterized functional EIT measures of time constant (71) and phase. Other functional measures have targeted Ventilation delay, and the delay of lung tissue opening and closing.

- *Tissue Classification*: Functional EIT measures have been used to classify lung tissue into various states. For example, regions of overdistention / atelectasis has been identified using the dynamic compliance and pressure time-course of the lungs. (36, 51).

- *Activation Patterns*: Functional EIT measures have also been proposed for brain EIT images. The pattern of activation within the cortex following stimulation has been analyzed using techniques such as optical flow techniques. (13)

- *Pulse Transit time*: The movement of pressure pulses in the vasculature is modulated by the blood pressure. This relationship has been used to measure both pulmonary- (77) (transit time from heart to lungs) and systemic-arterial pressure (transit time from heart to descending aorta) (87).

- *Blood flow (perfusion)*: To obtain measures of blood flow, it is possible to introduce EIT-contrast agents.

The main approach has been to inject a bolus of hypertonic saline (at 5-10× normal blood saline levels). This causes a region of much higher conductivity to move through the heart and vasculature. Using these data, EIT images of the blood flow through the heart and lungs(44), or brain(6) has been demonstrated.
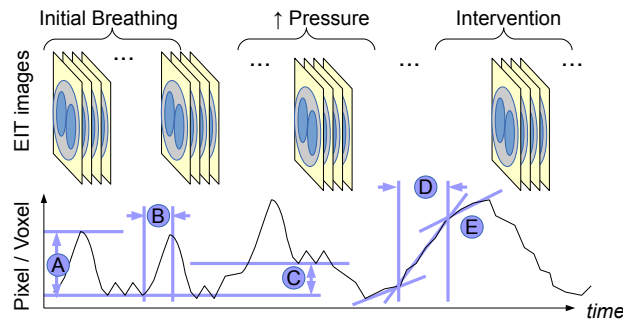
Figure 15: Overview of types of fEIT images, based on a scenario in which a mechanically ventilated patient starts at an initial pressure setting, which is subsequently increase, and finally subject to a slow inflation and deflation manoeuvre. Each letter indicates the type of fEIT images: A) measures of the distribution of ventilation and of regional compliance (the illustration shows a measure of tidal variation), B) measures of regional delays and time constants (the illustration shows a measure of inspiratory time), C) measures of regional changes in aeration due to an intervention (the illustration shows a slow inflation), and D) measures of manoeuvre timing, and E) measures of inflation and deflation parameters (the illustration shows maximum curvature-change points).

8 Discussion and Perspectives

This article reviews Electrical Impedance Tomography (EIT), a medical imaging technique which uses electrical current stimulations and measurements at body-surface electrodes to create images of the distribution of electrical impedivity (and its changes over time) within the body. EIT has seen proposed applications in many medical areas, from imaging lungs, heart and blood flow, brain and nerves, cancerous tissue and other applications.

Medical EIT is closely related to several other technologies which use impedance imaging, although these are typically referred to as ERT – electrical resistance tomography, and see use in geophysical imaging and process tomography. Geophysical imaging with electrical measurements has a long history (12). It is sensitive to the presence of conductive metallic ores and to conductive liquids in the soil. In the first application, ERT is used for mineral exploration, as well as for applications like archaeological surveys. For its sensitivity to ground water, ERT is used for monitoring of engineering structures

(embankments, bridging structures) which can fail when saturated. It is also used to monitor movement of polluted ground water (leach) from disposal sites, and for ground water movement.

Process tomography applications of ERT focus on monitoring of pipes and mixing vessels. In a flowing pipe, there is often a mixture of liquid, air and sediment. Under stable conditions, the sediment falls to the bottom and the air to the top with a layer of flowing liquid between. Under turbulent flow, these layers can mix or blockages can occur. ERT can usefully monitor these mixture layers. For mixing tanks, ERT is able to monitor the progressive mixing of constituents.

For medical applications, EIT is seeing an interesting transition from a largely research-only technique to early clinical use. There are now several companies which sell EIT systems to monitor ventilated patients, and EIT is becoming part of the hospital procurement cycle. In terms of publications, there is a strong and growing rate of citations of EIT in the medical literature. On the other hand, non-ventilation applications of EIT have not yet seen a transition to clinical use. We see a continued slow acceptance of EIT in the market for ventilation monitoring. In addition, EIT monitoring of infants offers significant advantages over other techniques, especially given the extremely sensitive skin of premature infants.

References

[1] M Abboud, R Guardo, R Martineau, J Taillefer, C Pelletier, "Monitoring of peripheral edema using electrical bioimpedance measurements" *Conf IEEE EMBS* pp 641–642, 1995.

[2] A Adler, R Guardo. "Electrical impedance tomography: regularized imaging and contrast detection." *IEEE T Medical Imag* 15:170–179, 1996.

[3] A Adler, WRB Lionheart "Uses and abuses of EIDORS: An extensible software base for EIT" *Physiol Meas* 27:S25–S42, 2006.

[4] A Adler, JH Arnold, R Bayford, A Borsic, B Brown, P Dixon, TJC Faes, I Frerichs, H Gagnon, Y Gärber, B Grychtol, G Hahn, WRB Lionheart, A Malik, RP Patterson, J Stocks, A Tizzard, N Weiler, GK Wolf "GREIT: a unified approach to 2D linear EIT reconstruction of lung images" *Physiol Meas*, 30:S35–S55, 2009

[5] A Adler, A Boyle, "Electrical Impedance Tomography: Tissue Properties to Image Measures", *IEEE T Biomed Eng*, 64:2494–2504, 2017

[6] A Adler, M Faulkner, K Aristovich, S Hannan, J Avery, DS Holder "Cerebral perfusion imaging using EIT", *Proc EIT 2017*, p.43, Dartmouth, NH, USA, June 21–24, 2017

[7] A Adler, MB Amato, JH Arnold, R Bayford, M Bodenstein, SH Böhm, BH Brown, I Frerichs, O Stenqvist, N Weiler, GK Wolf, "Whither lung EIT: where are we, where do we want to go, and what do we need to get there?" *Physiol Meas*, 33:679–694, 2012.

[8] A Adler, WRB Lionheart, "Conductivity perturbations in EIT" *Proc. Conf. EIT2016*, p 26, Neuchâtel, Switzerland, Jun 2–5, 2015.

[9] A Adler, R Gaburro, WRB Lionheart, "Electrical Impedance Tomography", in *Handbook of Mathematical Methods in Imaging*, 2nd ed O Scherzer (Ed), Springer, 2016.

[10] A Adler, A Boyle, WRB Lionheart "Efficient computations of the Jacobian matrix using different approaches are equivalent" *Proc. Conf. EIT2017*, p.74 Dartmouth, USA, Jun 21–24, 2017.

[11] A Adler, M Proença, F Braun, JX Brunner, J Solà, "Origins of Cardiosynchronous Signals in EIT", *Proc. Conf. EIT2017*, p.73 Dartmouth, USA, Jun 21–24, 2017.

[12] LA Allaud, MH Martin; "Schlumberger, the history of a technique", John Wiley and Sons, New York. 1977.

[13] KY Aristovich, GS dos Santos, BC Packham, DS Holder. "A method for reconstructing tomographic images of evoked neural activity with electrical impedance tomography using intracranial planar arrays", *Physiol meas*. 35:1095–1110, 2014.

[14] M Assenheimer, O Laver-Moskovitz, D Malonek, D Manor, U Nahaliel, R Nitzan, A Saad "The T-SCAN technology: electrical impedance as a diagnostic tool for breast cancer detection." *Physiol Meas* 22:1–8, 2001.

[15] DC Barber, BH Brown, IL Freeston; "Imaging Spatial distributions of resistivity using Applied Potential Tomography". *Electronics Letters* 19:93–95, 1983.

[16] MS Beck, RA Williams, "Process tomography: a European innovation and its applications" *Meas Sci Technol* 7:215–224, 1996

[17] M Bodenstein, M David, K Markstaller; "Principles of electrical impedance tomography and its clinical application." *Crit Care Med* 37:713–24, 2009.

[18] L Borcea; "Electrical impedance tomography." *Inverse Prob* 18:R99–R136, 2002.

[19] A Borsic, WR Lionheart, CN McLeod CN, "Generation of anisotropic-smoothness regularization filters for EIT. IEEE transactions on medical imaging." 21:579-587, 2002.

[20] A Borsic, R Halter R, Y Wan, A Hartov, KD Paulsen, "Sensitivity study and optimization of a 3D electric impedance tomography prostate probe" *Physiol Meas* 30:S1–S19, 2009.

[21] A Borsic, BM Graham, A Adler, WRB Lionheart, "In vivo Impedance Imaging with Total Variation Regularization", *IEEE T Medical Imaging* 29:44–54, 2010.

[22] A Borsic, A Adler, "A primal dual-interior point framework for using the L1-norm or the L2-norm on the data and regularization terms of inverse problems" *Inverse Prob*, 28:095011, 2012.

[23] F Braun, M Proença, J Solà, J-P Thiran, A Adler "A Versatile Noise Performance Metric for Electrical Impedance Tomography Algorithms" In press *IEEE T Biomed Eng* DOI:10.1109/TBME.2017.2659540

[24] F Braun, M Proença, A Adler, T Riedel, J-P Thiran, J Solà, "Accuracy and Reliability of Noninvasive Stroke Volume Monitoring via ECG-Gated 3D Electrical Impedance Tomography in Healthy Volunteers" *PLoS One*, 13:e0191870, 2018.

[25] BH Brown, AD Seagar, "The Sheffield data collection system", *Clin Phys Physiol Meas*, 8(Suppl A): 91–97, 1987.

[26] BH Brown; "Electrical impedance tomography (EIT): a review." *J Med Eng Technol* 27:97–108, 2003.

[27] AP Calderón, "On an inverse boundary value problem", in *Seminar on Numerical Analysis and its Applications to Continuum Physics*, Rio de Janeiro, Editors W.H. Meyer and M.A. Raupp, Sociedade Brasileira de Matematica, pp 65–73, 1980.

[28] H Caytak, A Boyle, A Adler, M Bolic, "Bioimpedance Spectroscopy Processing and Applications", In: *Reference Module in Biomedical Sciences*, Elsevier, 2017.

[29] M Cheney, D Isaacson, JC Newell, S Simske, J Goble. "NOSER: An algorithm for solving the inverse conductivity problem" *Int J Imag Syst Technol* 2:66–75, 1990.

[30] M Cheney, D Isaacson, JC Newell; "Electrical Impedance Tomography", SIAM Review, 41:85–101, 1999.

[31] KS Cheng, D Isaacson, JC Newell, DG Gisser DG, "Electrode models for electric current computed tomography", *IEEE T Biomed Eng* 36:918-924, 1989.

[32] V Cherepenin, A Karpov, A Korjenevsky, V Kornienko, A Mazaletskaya, D Mazourov, D Meister "A 3D electrical impedance tomography (EIT) system for breast cancer detection." *Physiol Meas* 22:9–18, 2001.

[33] MH Choi, TJ Kao, D Isaacson, GJ Saulnier, JC Newell "A reconstruction algorithm for breast cancer imaging with electrical impedance tomography in mammography geometry." *IEEE T Biomed Eng* 54:700-10, 2007.

[34] KS Cole, RH Cole, "Dispersion and absorption in dielectrics I: Alternating Current Characteristics", *J Chemical Physics* 9:341–351, 1941.

[35] EL Costa, RG Lima, MB Amato MB; "Electrical impedance tomography." *Curr Opin Crit Care* 15:18–24, 2009.

[36] EL Costa, JB Borges, A Melo, F Suarez-Sipmann, C Toufen Jr., SH Böhm, MB Amato "Bedside estimation of recruitable alveolar collapse and hyperdistension by electrical impedance tomography." *Int Care Med* 35:1132–1137, 2009.

[37] N Coulombe, H Gagnon, F Marquis, Y Skrobik, R Guardo "A parametric model of the relationship between EIT and total lung volume." *Physiol Meas* 26:401–411, 2005.

[38] PA Dargaville, PM Rimensberger, I Frerichs, "Regional tidal ventilation and compliance during a stepwise vital capacity manoeuvre" Intensive Care Med. 36:1953–1961, 2010.

[39] PJW Debye, *Polar Molecules*, p.172, The Chemical Catalog Company, Inc., 1929

[40] AM Dijkstra, BH Brown, AD Leathard, ND Harris, DC Barber, DL Edbrooke, "Review clinical applications of electrical impedance tomography" *J Medical Eng Technol*, 17:89–98, 1993.

[41] D Ferrario, B Grychtol, A Adler, J Sola, SH Böhm, M Bodenstein "Toward morphological thoracic EIT: major signal sources correspond to respective organ locations in CT" *IEEE T Biomed Eng* 59:3000–3008, 2012.

[42] KR Foster, HP Schawn, "Dielectric properties of tissues", pp 25–104 in C Polk, E Postow (eds), *Handbook of biological effects of electromagnetic fields, 2nd ed*, 1996.

[43] I Frerichs; "Electrical impedance tomography (EIT) in applications related to lung and ventilation: a review of experimental and clinical activities." *Physiol Meas* 21:R1–R21, 2000.

[44] I Frerichs, J Hinz, P Herrmann, G Weisser, G Hahn, M Quintel, G Hellige. "Regional lung perfusion as determined by electrical impedance tomography in comparison with electron beam CT imaging" *IEEE T Med Imag* 21:646–652, 2002.

[45] I Frerichs, PA Dargavillle, T Dudykevych, PM Rimensberger, "Electrical Impedance Tomography – a method for monitoring regional lung aeration and tidal volume distribution?", *Int Care Med* 29:2312–2316, 2003.

[46] I Frerichs, T Becher, N Weiler; "Electrical impedance tomography imaging of the cardiopulmonary system." *Curr Opin Crit Care* 20:323–32, 2014.

[47] I Frerichs, M Amato, A Van Kaam, D Tingay, Z Zhao, B Grychtol, M Bodenstein, H; Gagnon, S Böhm, E Teschner, O Stenqvist, T Mauri, V Torsani, C Luigi, A Schibler, G Wolf, D Gommers, S Leonhardt, A Adler "Chest electrical impedance tomography examination, data analysis, terminology, clinical use and recommendations: consensus statement of the TRanslational EIT developmeNt stuDy group" *Thorax*, 72:83–93, 2017.

[48] S Gabriel, RW Lau, C Gabriel, "The dielectric properties of biological tissues: III. Parametric models for the dielectric spectrum of tissues", *Phys Med Biol* 41:2271–2293, 1996.

[49] C Gabriel, A Peyman, EH Grant, *Electrical conductivity of tissue at frequencies below 1 MHz Phys Med Biol* 54:4863–4878, 2009.

[50] RL Gaw, *The effect of red blood cell orientation on the electrical impedance of pulsatile blood with implications for impedance cardiography PhD Thesis*, Queensland University of Technology, 2010.

[51] C Gómez-Laberge, JH Arnold, GK Wolf "A Unified Approach for EIT Imaging of Regional Overdistension and Atelectasis in Acute Lung Injury", *IEEE T Medical Imag*, 31:834–842, 2012.

[52] B Grychtol, A Adler, "FEM electrode refinement for Electrical Impedance Tomography" *Conf IEEE EMBS* pp 6429–6432, 2013.

[53] RJ Halter, A Hartov, JA Heaney, KD Paulsen, AR Schned "Electrical impedance spectroscopy of the human prostate." *IEEE T Biomed Eng* 54:1321-7, 2007.

[54] Hahn G, Šipinková I, Baisch F, Hellige G. "Changes in the

thoracic impedance distribution under different ventilatory conditions", *Physiol Meas* 16:A161–173, 1995.

[55] PC Hansen, DP O'Leary "The Use of the L-Curve in the Regularization of Discrete Ill-Posed Problems" *SIAM J Sci Comput*, 14:1487–1503, 1993

[56] S Heinrich, H Schiffmann, A Frerichs, A Klockgether-Radke, I Frerichs, "Body and head position effects on regional lung ventilation in infants: an electrical impedance tomography study". *Intensive Care Med*, 32:1392–1398, 2006.

[57] RP Henderson, JG Webster; "An Impedance Camera for Spatially Specific Measurements of the Thorax" *IEEE T Biomed Eng* 25:250–254, 1978.

[58] DS Holder, "Electrical impedance tomography with cortical or scalp electrodes during global cerebral ischaemia in the anaesthetised rat." *Clin Phys Physiol Meas* 13:87–98, 1992.

[59] DS Holder, ed; "Electrical impedance tomography: methods, history and applications." CRC Press, 2004.

[60] IEC 60601-1:2015, "Medical Electrical Equipment Part 1: General Requirements for Basic Safety and Essential Performance", Brussels: International Electrotechnical Commission, 2015

[61] J Jossinet, "The impedivity of freshly excised human breast tissue" *Physiol Meas* 19:61–75, 1998.

[62] J Larsson, "Electromagnetics from a quasistatic perspective", *Am J Physics* 75:230-239, 2007.

[63] S Leonhardt, A Cordes, H Plewa, R Pikkemaat, I Soljanik, K Moehring, HJ Gerner, R Rupp, "Electric impedance tomography for monitoring volume and size of the urinary bladder." *Biomedizinische Technik* 56:301–307, 2011

[64] S Leonhardt, B Lachmann; "Electrical impedance tomography: the holy grail of ventilation and perfusion monitoring?" *Int Care Med* 38:1917-1929, 2012.

[65] WRB Lionheart, J Kaipio, CN McLeod; "Generalized optimal current patterns and electrical safety in EIT." *Physiol Meas* 22: 85–90, 2001.

[66] HA Lorentz, "The theorem of Poynting concerning the energy in the electromagnetic field and two general propositions concerning the propagation of light" *Amsterdammer Akademie der Wetenschappen* 4:176–187, 1896.

[67] S Lundin, O Stenqvist; "Electrical impedance tomography: potentials and pitfalls." *Curr Opin Crit Care* 18:35–41, 2012.

[68] Y Mamatjan, B Grychtol, P Gaggero, J Justiz, V Koch, A Adler. "Evaluation and Real-Time Monitoring of Data Quality in Electrical Impedance Tomography". *IEEE T Med Imaging* 32:1997–2005, 2013.

[69] YF Mangnall, AJ Baxter, R Avill, NC Bird, BH Brown, DC Barber, AD Seagar, AG Johnson, NW Read "Applied potential tomography: a new noninvasive technique for assessing gastric function", *Clin Phys Physiol Meas*, 8:119-129 1987.

[70] JC Maxwell Garnett, "Colours in metal glasses, in metallic films, and in metallic solutions II", *Phil Trans Royal Society A*, 205:387–401, 1906.

[71] M Miedema, FH de Jongh, I Frerichs, MB van Veenendaal, AH van Kaam. "egional respiratory time constants during lung recruitment in high-frequency oscillatory ventilated preterm infants" *Int Care Med* 38:294–299, 2012

[72] Miedema M *et al*, "First Real-Time Visualization of a Spontaneous Pneumothorax Developing in a Preterm Lamb Using Electrical Impedance Tomography", *Am J RCCM*, 194:116–118, 2016.

[73] D Miklavčič, N Pavšelj, FX Hart, "Electric Properties of Tissues", In: *Wiley Encyclopedia of Biomedical Engineering*, Wiley, 2006

[74] JC Newell, PM Edic, X Ren, JL Larson-Wiseman, MD Danyleiko, "Assessment of acute pulmonary edema in dogs by electrical impedance imaging." *IEEE T Biomed Eng* 43:133–138, 1996.

[75] DT Nguyen, C Jin, A Thiagalingam, AL McEwan "A review on electrical impedance tomography for pulmonary perfusion imaging." *Physiol Meas* 33:695–706, 2012.

[76] N Polydorides, WRB Lionheart. "A Matlab toolkit for three-dimensional electrical impedance tomography: a contribution to the Electrical Impedance and Diffuse Optical Reconstruction Software project." *Meas Sci Technol* 13:1871–1883, 2002.

[77] M Proença, F Braun, J Solà, A Adler, M Lemay, J-P Thiran, SF Rimoldi "Non-invasive monitoring of pulmonary artery pressure from timing information by EIT: experimental evaluation during induced hypoxia" *Physiol Meas* 37:713–726, 2016.

[78] S Pulletz, A Adler, M Kott, G Elke, B Gawelczyk, D Schädler, G Zick, N Weiler, I Frerichs "Regional lung opening and closing pressures in patients with acute lung injurys", *J Critical Care*, 27:3:323.e11–323.e18, 2012.

[79] S Pulletz, M Kott, G Elke, D Schadler, B Vogt, N Weiler, I Frerichs "Dynamics of regional lung aeration determined by electrical impedance tomography in patients with acute respiratory distress syndrome", *Multidiscip Respir Med* 7:44, 2012.

[80] A Rao, A Gibson, D Holder. "EIT images of electrically induced epileptic activity in anaesthetised rabbits", *Med Biol Engin Comput* 35:327, 1997.

[81] T Riedel, I Frerichs; "Electrical impedance tomography." *Eur Respir Mon* 47:195–205, 2010.

[82] A Romsauerova, A McEwan, L Horesh, R Yerworth, RH Bayford, DS Holder "Multi-frequency electrical impedance tomography (EIT) of the adult human head: initial findings in brain tumours, arteriovenous malformations and chronic stroke, development of an analysis method and calibration." *Physiol Meas* 27:S146–S161, 2006.

[83] RJ Sadleir, T Tang, AS Tucker, P Borum, M Weiss "Detection of intraventricular blood using EIT in a neonatal piglet model." *Conf IEEE EMBS* pp 3169-3172, 2009.

[84] A Schibler, TMT Pham, AA Moray, C Stocker "Ventilation and cardiac related impedance changes in children undergoing corrective open heart surgery" Physiol Meas, 34:1319–1327, 2013.

[85] JK Seo, J Lee, SW Kim, H Zribi, EJe Woo; "Frequency-difference electrical impedance tomography (fdEIT): algorithm development and feasibility study", *Physiol Meas* 29:929–944, 2008.

[86] HJ Smit, ML Handoko, A Vonk Noordegraaf, TJ Faes, PE Postmus, PM de Vries, A Boonstra "Electrical impedance tomography to measure pulmonary perfusion: Is the reproducibility high enough for clinical practice?" *Physiol Meas* 24:491-499, 2003.

[87] J Solà, A Adler, A Santos, G Tusman, FS Sipmann, SH Böhm, "Non-invasive monitoring of central blood pressure by Electrical Impedance Tomography (EIT): first experimental evidence" *Med Biol Eng Comput*, 49:409–415, 2011.

[88] Soleimani M, "Electrical impedance tomography imaging using a priori ultrasound data." *Biomedical engineering online* 5, 2006. DOI:10.1186/1475-925X-5-8

[89] J Sylvester, G Uhlmann, "A uniqueness theorem for an inverse boundary value problem n electrical prospection" *Comm Pure Appl Math* 3991-3112, 1986.

[90] A Tamburrino, G Rubinacci, "A new non-iterative in version method in electrical resistance tomography", *Inverse Prob*, 18:1809-1829, 2002.

[91] CJC Trepte, CR Phillips, J Solà, A Adler, SA Haas, M Rapin; SH Böhm, DA Reuter "Electrical impedance tomography (EIT) for quantification of pulmonary edema in acute lung injury", *Crit Care*, 20:18, 2016.

[92] CJC Trepte, C Phillips, J Solà, A Adler, B Saugel, S Haas, SH Böhm, DA Reuter "Electrical impedance tomography (EIT) for non-invasive assessment of stroke volume variation in health and experimental lung injury" *Br J Anaesthesia*, 118:68–76, 2017.

[93] Y Wan, A Borsic, J Heaney, J Seigne, A Schned, M Baker, S Wason, A Hartov, R Halter "Transrectal electrical impedance tomography of the prostate: Spatially coregistered pathological findings for prostate cancer detection" *Medical physics* 40:063102, 2013.

[94] TJ Yorkey, JG Webster, WJ Tompkins, "Comparing reconstruction algorithms for electrical impedance tomography" *IEEE T Biomed Eng* 11:843–852, 1987.